한국전산구조공학회
2002년도 봄 학술발표회 논문집

다중 셀 단면을 갖는 박판 복합재료 블레이드의 구조해석에 관한 연구

Structural Analysis of Thin-walled Composite Blades with Multi-cell Sections

정 성 남* 이 주 영** 박 일 주**
Jung, Sung-Nam Lee, Ju-Young Park, Il-Ju

초 록

본 연구에서는 임의의 형상의 다중세포 단면을 갖는 복합재료 블레이드에 대한 유한요소 구조해석을 수행하였다. 보 해석 모델은 구조연성 효과와 단면 벽의 두께, 횡 전단변형, 비틀림과 연관된 워핑 및 워핑구속효과 등을 고려하고 있다. 블레이드 힘-변위 관계식은 Reissner의 반보족에너지 함수를 이용한 혼합이론을 적용하여 유도하였다. 이 관계식은 굽힘 및 전단에 대해서는 Timoshenko 보의 형태로 그리고 비틀림 변형은 Vlasov 이론으로 근사하고 있다. 결과적인 [7x7] 구조강성 행렬은 전단변형 및 전단강성계수들을 특이한 가정에 의존하지 않고도 해석적으로 기술하고 있다. 본 정식화 과정을 통해서 구한 보 이론을 이중세포로 구성된 에어포일 형상의 복합재료 블레이드에 적용하였으며, 기존의 실험 연구 및 다차원 유한요소해석 결과들과 비교 연구를 수행하여 본 해석모델의 타당성을 보이고자 하였다.

1. Introduction

There have been a few selected research activities to model and analyze composite beams and blades with multi-cell sections. Mansfield[1] developed a flexibility formulation for thin-walled composite beams with two-cell cylindrical tube section. The equilibrium equations of shell wall were used to derive the (4x4) flexibility matrix that captures the classical four beam variables (extension, bendings in two planes, and torsion). Volovoi and Hodges[2] used the variational asymptotic approach to derive the asymptotically correct (4x4) stiffness matrix for thin-walled anisotropic beams with single- and double-celled box sections. Numerical results were presented to show the importance of incorporating shell bending strain measures even for closed thin-walled cross sections in the beam formulation. Chandra and Chopra[3] investigated both analytically and experimentally the structural response of two-cell composite blades with extension-torsion couplings. The stiffness matrix derived was of the order of (9x9) since they include derivatives of shear strains as independent variables in order to include transverse shear couplings in their formulation.

Recently, Jung, et al.[4] developed a mixed beam theory that takes into account the effects of elastic couplings, transverse shear deformation, warping, warping restraint, and bending and shear of the shell wall. The term mixed was used because of the fact that the direct stresses are treated as the known variables in terms of assumed displacements while the shear flow and hoop moment in the shell wall are treated as the unknown. The resulting (7x7) stiffness matrix characterizes elastic properties of the beam in terms of the axial, flap and lag bending, flap and lag shear, torsion, and torsion-warping deformations.

* 정회원 · 전북대학교 기계항공시스템 공학부 부교수
** 전북대학교 대학원 석사과정

The theory was applied to open and closed (single-cell) cross-section beams and a good correlation was achieved in comparison with experimental test data.

In the present work, the mixed formulation developed in Ref. 4 has been applied to analyze coupled composite beams and blades with single-cell box sections and two-cell airfoil. The formulation is validated by comparison of the values of cross-sectional properties and steady response of multi-celled section blades with experimental results and results from existing analysis methods found in the literature.

2. Formulation

Fig.1 shows the geometry and generalized forces for a composite blade with arbitrary cross-section. Two systems of coordinate axes are used: an orthogonal Cartesian coordinate system (x, y, z) for the blade; a curvilinear coordinate system (x, s, n) for the shell wall of the section. The global deformations of the beam are (U, V, W) along the x, y and z axes, and ϕ is the twist about the x-axis. The local shell deformations are (u, v_t, v_n) along the x, s and n directions, respectively. Allowing the transverse shear deformations, the local deformations at an arbitrary point on the shell wall can be expressed as

$$u = u^0 + n\Psi_x \quad ; \quad ;\nu_t = v_t^0 + n\Psi_s \quad ; \quad \nu_n = \nu_n^0 \tag{1}$$

In Eq. (1), u^0, ν_t^0 and ν_n^0 represent the deformations at the mid-plane of the shell wall and Ψ_x, Ψ_s represent rotations of the normals to the mid-plane about the s- and x- axes, respectively. The shell mid-plane displacements can be obtained in terms of the beam displacements and rotations as:

$$\nu_t^0 = Vy_{,s} + Wz_{,s} + r\phi \quad ; \quad \nu_n^0 = Vz_{,s} - Wy_{,s} - q\phi \quad ; \quad \Psi_s = \phi \tag{2}$$

where r and q are the coordinates of an arbitrary point on the shell wall in the (n, s) coordinate system. The cross-section rotations β_y and β_z are defined as:

$$\beta_y = \gamma_{xz} - W_{,x} \quad ; \quad \beta_z = \gamma_{xy} - V_{,x} \tag{3}$$

Using Eq. (1) through Eq. (2), the strain-displacement relation of the shell wall can be obtained as:

$$\begin{aligned} &\epsilon_{xx} = U_{,x} + z\beta_{y,x} + y\beta_{z,x} - \bar{\omega}\phi_{,xx} \quad ; \quad \gamma_{xs} = u_{,s}^0 + V_{,x}y_{,s} + W_{,x}z_{,s} + r\phi_{,x} \\ &\varkappa_{xx} = \beta_{z,x}z_{,s} - \beta_{y,x}y_{,s} + q\phi_{,xx} \quad ; \quad \varkappa_{xs} = 2\phi_{,x} \end{aligned} \tag{4}$$

where $\bar{\omega}$ is the sectorial area.[4]

Assuming the hoop stress flow N_{ss} is negligibly small and partially inverting the constitutive relations for the shell wall of the section one can express the relations into the following form.[4]

$$\begin{Bmatrix} N_{xx} \\ M_{xx} \\ M_{xs} \\ \gamma_{xs} \\ \varkappa_{ss} \end{Bmatrix} = \begin{bmatrix} C_{n\varepsilon} & C_{nx} & C_{n\phi} & C_{n\gamma} & C_{n\tau} \\ C_{nx} & C_{mx} & C_{m\phi} & C_{m\gamma} & C_{m\tau} \\ C_{n\phi} & C_{m\phi} & C_{\phi\phi} & C_{\phi\gamma} & C_{\phi\tau} \\ -C_{n\gamma} & -C_{m\gamma} & -C_{\phi\gamma} & C_{\gamma\gamma} & C_{\gamma\tau} \\ -C_{n\tau} & -C_{m\tau} & -C_{\phi\tau} & C_{\gamma\tau} & C_{\tau\tau} \end{bmatrix} \begin{Bmatrix} \epsilon_{xx} \\ \varkappa_{xx} \\ \varkappa_{xs} \\ N_{xs} \\ M_{ss} \end{Bmatrix} \tag{5}$$

or in symbolic notation

$$\{s\} = [C]\{e\} \tag{5a}$$

In order to assess the semi-inverted constitutive relations (5) into the beam formulation, a modified form of Reissner's semi-complimentary energy functional Φ_R is introduced:

$$\Phi_R = \frac{1}{2}[N_{xx}\epsilon_{xx} + M_{xx}\varkappa_{xx} + M_{xs}\varkappa_{xs} - N_{xs}\gamma_{xs} - M_{ss}\varkappa_{ss}] \tag{6}$$

The stiffness matrix relating beam forces to beam displacements is obtained by using the variational statement of the Reissner functional which is given by

$$\delta\int_0^l\int_C\left\{\Phi_R+\gamma_{xs}N_{xs}+\varkappa_{ss}M_{ss}+\frac{1}{2}N_{xs}(\gamma_{xs}-u_{,s}-\nu_{t,x})\right\}dsdx=0 \tag{7}$$

where l is the length of the blade. Performing the integrals, Eq. (7) results in the equilibrium equations of an element of the shell wall as well as the constraint conditions, which are found as:

$$\begin{array}{lll} N_{xx,x}+N_{xs,s}=0 & ; & N_{xs,x}=0 \\ M_{xx,x}+M_{xs,s}=0 & ; & M_{xs,x}+M_{ss,s}=0 \\ \gamma_{xs}-u^0_{,s}-\nu_{t,x}=0 & ; & \varkappa_{ss}-\Psi_{s,s}=0 \end{array} \tag{8}$$

The first two equations in Eq. (8) indicate that N_{xs} consists of a constant part and a part that depends on the s-integral of $N_{xx,x}$. In addition, it is found from the third and fourth equations in Eq. (8) that M_{ss}. has a constant part, a part that varies linearly with s and a part that depends on the s -integral of $M_{xs,x}$. Hence, one can write

$$\begin{aligned} N_{xs}&=N^0_{xs}-\int_0^s(A'_{11}\varepsilon_{xx,x}+B'_{16}\varkappa_{xs,x})ds \\ M_{ss}&=M^0_{ss}+yM^y_{ss}+zM^z_{ss}-\int_0^s(B'_{16}\varepsilon_{xx,x}+D'_{16}\varkappa_{xs,x})ds \end{aligned} \tag{9}$$

where $N^0_{xs}, M^0_{ss}, M^y_{ss}, M^z_{ss}$ represent the circuit shear flows for each cell of a closed multi-cell section. For a two-cell blade, these lead to eight unknowns which are expressed as:

$$\{n\}=\lfloor\ n_1\ n_2\ m_1\ m_2\ m_1^y\ m_2^y\ m_1^z\ m_2^z\ \rfloor^T \tag{10}$$

The continuity condition that must be satisfied for each wall of the section yields the following sets of equations

$$\begin{array}{llll} \oint_I\gamma_{xs}ds=2A_1\phi_{,x}\ , & \oint_I\varkappa_{xs}ds=0\ , & \oint_I y\varkappa_{xs}ds=0\ , & \oint_I z\varkappa_{xs}ds=0 \\ \oint_{II}\gamma_{xs}ds=2A_2\phi_{,x}\ , & \oint_{II}\varkappa_{xs}ds=0\ , & \oint_{II}y\varkappa_{xs}ds=0\ , & \oint_{II}z\varkappa_{xs}ds=0 \end{array} \tag{11}$$

where the subscripts I and II indicate integration over the contour of cells I and II, respectively (see Fig. 2). Inserting Eq. (5) into Eq. (11), the unknown shear flows can be obtained as:

$$\{n\}=[Q]^{-1}\cdot([P]\{\bar{q}_b\}+[R]\{\bar{q}_{b,x}\})=[b]\{\bar{q}_b\}+[B]\{\bar{q}_{b,x}\} \tag{12}$$

where

$$\{\bar{q}_b\}=\lfloor\ U_{,x}\ \beta_{y,x}\ \beta_{z,x}\ \phi_{,x}\ \phi_{,xx}\ \rfloor^T \tag{13}$$

In Eq. (12), $[Q]$ is a symmetric (8×8) matrix and $[P]$ is a (8×5) matrix. Note that these matrices are integrals over the contour and do not contain any coordinates such as y, z or s. If Eq. (12) is used, the shear flow and the hoop moment, Eq. (9), can be expressed as

$$\begin{Bmatrix} N_{xs} \\ M_{ss} \end{Bmatrix}\equiv\{\xi\}=\{\xi^a\}+\{\xi^r\}=[f]\{\bar{q}_b\}+[F]\{\bar{q}_{b,x}\} \tag{14}$$

It is noted that N_{xs} and M_{ss} should be determined separately for each cell. The shear flow components N_{xs} and M_{ss} are thought of as composed of an active and a reactive part according to the terminology introduced in Gjelsvik.[5] The superscripts a and r appeared in Eq. (14) reflect this aspect.

Using Eq. (5a), the Reissner statement (Eq. (7)) can be rewritten as

$$\delta\int_0^l\int_C\frac{1}{2}\left[\{e_1\}^T[C]\{e_1\}+2\{\xi^a\}^T[\Lambda]\{\xi^r\}+\{\xi^r\}^T[\Lambda]\{\xi^r\}+N_{xs}(\gamma_{xs}-u_{,s}-\nu_{t,x})\right]dsdx=0 \tag{15}$$

where

$$\begin{aligned} \{e_1\}&=\lfloor\ \varepsilon_{xx}\ \varkappa_{xx}\ \varkappa_{xs}\ N^a_{xs}\ M^a_{ss}\ \rfloor^T \\ [\Lambda]&=\begin{bmatrix} C_{\gamma\gamma} & C_{\gamma\varkappa} \\ C_{\varkappa\gamma} & C_{\varkappa\varkappa} \end{bmatrix} \end{aligned} \tag{16}$$

The first term in Eq. (15) can be written in terms of beam displacements by using Eqs. (4) and (14),

$$\delta\int_0^l\int_C\frac{1}{2}\{\bar{q}_b\}^T[T]^T[C][T]\{\bar{q}_b\}dsdx=\delta\int_0^l\frac{1}{2}\{\bar{q}_b\}^T[\hat{R}_{bb}]\{\bar{q}_b\}dx \tag{17}$$

where

$$[T]=\begin{bmatrix}1 & z & y & 0 & -\bar{\omega}\\ 0 & -y_{,s} & z_{,s} & 0 & q\\ 0 & 0 & 0 & 2 & 0\\ f_x & f_y & f_z & f_\phi & f_\omega\\ g_x & g_y & g_z & g_\phi & g_\omega\end{bmatrix} \tag{18}$$

The cross-section stiffness matrix $[\hat{R}_{bb}]$ relates the cross-section force and moment resultants with beam displacements in an Euler-Bernoulli level of approximation and is given by:

$$\{\bar{F}_b\}\lfloor N\ M_y\ M_z\ T\ M_\omega\rfloor^T=[\hat{R}_{bb}]\{\bar{q}_b\} \tag{19}$$

where N is the axial force, M_y and M_z are bending moments about y and z directions, respectively, T is the twisting moment and M_ω is the Vlasov bi-moment. In order to obtain the equivalent of a Timoshenko theory for the blade, we consider a cantilevered blade loaded at the tip with shear forces V_y and V_z . Differentiating Eq. (19) with respect to x, we obtain

$$\{\bar{F}_{b,x}\}=\lfloor 0\ V_z\ V_y\ 0\ 0\rfloor^T=[\hat{R}_{bb}]\{\bar{q}_{b,x}\} \tag{20}$$

Considering Eqs. (14) and (20), one can obtain the reactive part of the shear flow $\{\xi^r\}$ as

$$\{\xi^r\}=[F][\hat{R}_{bb}]^{-1}\{\bar{F}_{b,x}\}=\begin{bmatrix}f_y^r & f_z^r\\ g_y^r & g_z^r\end{bmatrix}\begin{Bmatrix}V_y\\ V_z\end{Bmatrix}\equiv[f^r]\{\bar{v}_s\} \tag{21}$$

Combining this result with Eq. (17), Eq. (15) yields the following equation:

$$\delta\frac{1}{2}\int_0^l\lfloor\bar{q}_b\ \bar{v}_s\rfloor\begin{bmatrix}\hat{R}_{bb} & \hat{R}_{bv}\\ \hat{R}_{bv}^T & \hat{R}_{vv}\end{bmatrix}\begin{Bmatrix}\bar{q}_b\\ \bar{v}_s\end{Bmatrix}dx+\delta\frac{1}{2}\int_0^l\oint N_{xs}(\gamma_{xs}-u_{,s}-v_{l,x})dsdx=0 \tag{22}$$

where

$$\begin{aligned}\lfloor\hat{R}_{bv}\rfloor &= [f]^T[\Lambda]\lfloor f^r\rfloor\\ [\hat{R}_{vv}] &= [f^r]^T[\Lambda][f^r]\end{aligned} \tag{23}$$

V_y and V_z are determined such that Eq. (22) is satisfied. Inserting Eqs. (4) and (5) into the second part of Eq. (22), the shear forces $\{\bar{v}_s\}$ can be related with beam displacement vector $\{q\}$ as:

$$\{\bar{v}_s\}=[P]\{q\} \tag{24}$$

where

$$\{q\}=\lfloor U_{,x}\ \beta_{y,x}\ \beta_{z,x}\ \phi_{,x}\ \phi_{,xx}\ \gamma_{xy}\ \gamma_{xz}\rfloor^T \tag{25}$$

The elements of the (2×7) matrix $[P]$ in Eq. (24) are the same as those obtained using the first order shear deformation theory with shear correction factors of unity. By comparing Eq. (22) with Eq. (24) we get:

$$\begin{Bmatrix}\bar{q}_b\\ \bar{v}_s\end{Bmatrix}=\begin{bmatrix}[I_{5\times5}] & [O_{5\times2}]\\ [p_1] & [p_2]\end{bmatrix}\{q\} \tag{26}$$

where $[I_{5\times5}]$ is a (5×5) identity matrix and $[0_{5\times5}]$ is a null matrix of size (5×2), while $[p_1]$ has a size of (2×5) and $[p_2]$ has a dimension of (2×2). Using Eq. (26), the first part of Eq. (22) yields the following form:

$$\int_0^l\lfloor\delta\bar{q}_b\ \delta\bar{v}_s\rfloor\begin{bmatrix}\hat{R}_{bb} & \hat{R}_{bv}\\ \hat{R}_{bv}^T & \hat{R}_{vv}\end{bmatrix}\begin{Bmatrix}\bar{q}_b\\ \bar{v}_s\end{Bmatrix}dx=\int_0^l\{\delta q\}^T[\bar{K}]\{q\}dx \tag{27}$$

where the (7×7) stiffness matrix $[K]$ is given by

$$[\overline{K}]=\begin{bmatrix}\overline{K}_{bb} & \overline{K}_{bv}\\ \overline{K}_{bv} & \overline{K}_{vv}\end{bmatrix}=\begin{bmatrix}\{\hat{K}_{bb}+2\hat{K}_{bv}p_1+p_1^T\hat{K}_{vv}p_1\} & \{\hat{K}_{bv}p_2+p_1^T\hat{K}_{vv}p_2\}\\ \{\hat{K}_{bv}p_2+p_1^T\hat{K}_{vv}p_2\} & \{p_2^T\hat{K}_{vv}p_2\}\end{bmatrix} \tag{28}$$

The stiffness matrix $[\overline{K}]$ in Eq. (28) represents the idealization of the blade at a Timoshenko level for bending and shear, while the torsion is idealized as the Vlasov torsion.

The finite element equations are obtained by applying the stationary potential energy theorem. The potential energy of the beam as written as:

$$\Pi=\frac{1}{2}\int_0^l\{q_b\}^T\{F_b\}dx-\frac{1}{2}\int_0^l\{q_b\}^T\{f_c\}dx \tag{29}$$

where F_b is the generalized force vector, $\{q_b\}$ is the corresponding deformations and $\{f_c\}$ is the generalized load vector. Inserting Eq. (28) into Eq. (29) and applying a variational statement yields the following equation

$$\delta\Pi=\int_0^l\{\delta q_b\}^T[\overline{K}]\{q_b\}dx-\int_0^l\{\delta q_b\}^T\{f_c\}dx \tag{30}$$

Three different types of shape functions are introduced to describe the behavior of the beam. For the axial displacement U, a four-node Lagrangian representation is used. The cross-section rotations (β_y and β_z) and the transverse deformation (V and W) are interpolated using a three-node Lagrangian shape function. For twist deformation ϕ and its derivative $\phi_{,x}$, a two-node Hermite shape function is employed to satisfy the C^1-continuity at each extremities of an element. These yield a total of 20 degrees of freedom for each finite element. Considering these finite element representation into the energy expression Eq. (30), we obtain the following set of finite element beam equations:

$$[K]\{q_G\}=\{F_G\} \tag{31}$$

where $[K]$ and $\{F_G\}$ are the finite element system of stiffness matrix and load vector, respectively, and $\{q_G\}$ is the generalized displacement vector for the beam.

3. Results and Discussions

Numerical simulations are carried out for coupled composite blades with two-cell airfoil section. Fig. 2 shows the schematic of the two-cell blade section fabricated and tested by Chandra and Chopra.[3] The blade is clamped at one end and warping restrained at both ends. The geometry and the material properties of the blade are given in Table 1. Blades with three different ply layups representing bending-torsion couplings are studied. Table 2 shows the details of the layup used in the blades.

Fig. 3 shows the comparison results for the tip bending slope and induced tip twist of the bending-torsion coupled blade (Blade 1) under unit tip bending load. As is given in Table 2, Blade 1 consists of 15° spar and ±15° skin. The present results are compared with the experimental test data as well as the theoretical results obtained by Chandra and Chopra.[3] As can be seen in Fig. 3, the predictions of the present method are in good agreement with experimental results. The responses obtained by the present method are within 4.5% of the test results. The difference between the current predictions and Ref. 3 is due mainly to the fact that Chandra and Chopra[3] used the zero-in-plane strain assumption ($\gamma_{ss}=\varkappa_{ss}=0$) for the constitutive relations, while in the present approach, the zero hoop stress flow assumption ($N_{ss}=0$) is used. Fig. 4 presents the tip twist and induced bending slope for Blade 1 under unit tip torsional load. There is a good correlation between the present theory and

experimental results.

Figs. 5 and 6 show the structural responses of the 30° blade (Blade 2) under unit tip bending and torsional loads, respectively. The present predictions are seen to be in a good agreement with experimental results. The error is within 7% of the test results. The results obtained by the present mixed method show better correlations with the experimental results than those obtained by the stiffness method of Chandra and Chopra[3]. Figs. 7 and 8 show results of Blade 3 which has ply angles of 45 degrees. For this blade also, the predicted responses are within 5% of the experimental results. Note the increase in bending slope (over 30%) and decrease in induced twist (over 50%) for this blade in comparison with the previous blades (Blade 1 and 2). The decrease in bending stiffness with respect to the increase in ply angles causes this aspect. The existence of bending-torsion couplings reduces the direct bending stiffness in some degree.

4. Concluding Remarks

In the present work, a closed-form formulation for coupled composite blades with multiple cell sections has been developed. The analysis model includes the effects of elastic couplings, shell wall thickness, transverse shear deformation, torsion warping and constrained warping. The beam force-displacement relations of the blade were obtained by using the Reissner's semi-complementary energy functional. The resulting (7x7) stiffness matrix idealizes the blade at a Timoshenko level of approximation for bending and shear and Vlasov for torsion. It is shown that the elements of the stiffness matrix are modified by the shear related terms and shear correction terms. The theory has been correlated with experimental test data and detailed finite element results for coupled composite beams and blades with single-cell box-sections and two-cell airfoils. Good correlation of responses with experimental results was obtained for all the test cases considered. The error is less than 7% for bending-torsion coupled blades.

Acknowledgement

This work was supported from the Basic Research Program (Grant No.: 2001-1-30500-001-2) by the Korea Science and Engineering Foundation.

References

1. Mansfield, E. H., "The Stiffness of a Two-Cell Anisotropic Tube," *Aeronautical Quarterly*, May 1981, pp. 338-353.
2. Volovoi, V. V., and Hodges, D. H., "Single- and Double-Celled Composite Thin-Walled Beams," *Proceedings of the 41st Structures, Structural Dynamics, and Materials Conference*, Atlanta, GA, Apr. 3-6, 2000, AIAA Paper 2000-1537.
3. Chandra, R., and Chopra, I., "Structural Response of Composite Beams and Blades with Elastic Couplings," *Composites Engineering*, Vol. 2, Nos. 5-7, 1992, pp. 347-374.
4. Jung, S. N., Nagaraj, V. T., and Chopra, I., "Refined Structural Model for Thin- and Thick-Walled Composite Rotor Blades," *AIAA Journal*, Vol. 40, No. 1, Jan. 2002, pp. 105-116.
5. Gjelsvik, A., *The Theory of Thin Walled Bars*, John Wiley & Sons, Inc., 1981

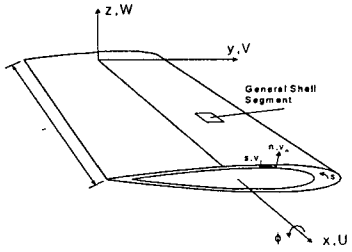

Fig. 1 Geometry and coordinate systems.

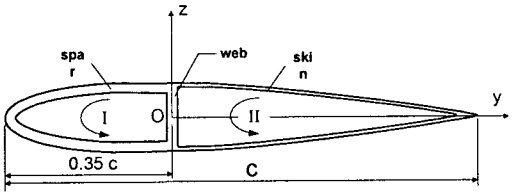

Fig. 2 Schematic of a two-cell airfoil section.

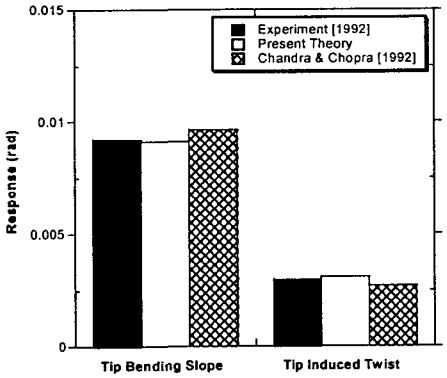

Fig. 3 Comparison of response for bending-torsion coupled blades (Blade 1) under unit tip bending load.

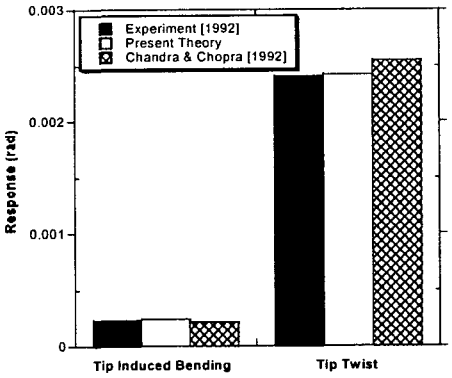

Fig. 4 Comparison of response for bending-torsion coupled blades (Blade 1) under unit tip torque load.

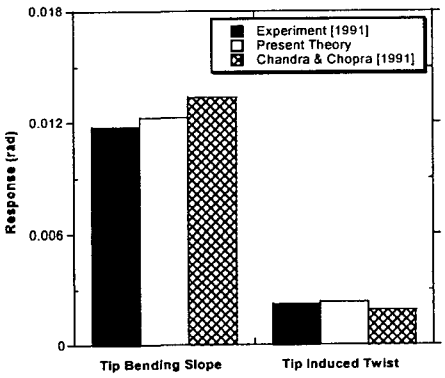

Fig. 5 Comparison of response for bending-torsion coupled blades (Blade 2) unit tip bending load.

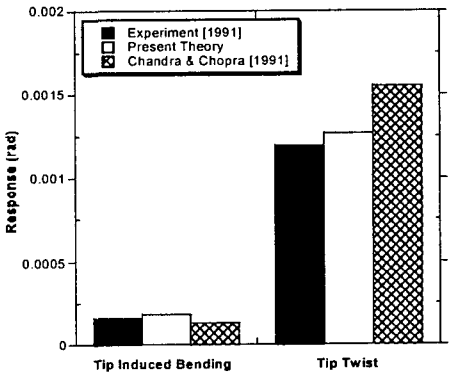

Fig. 6 Comparison of response for bending-torsion coupled blade (Blade 2) under unit tip torque load

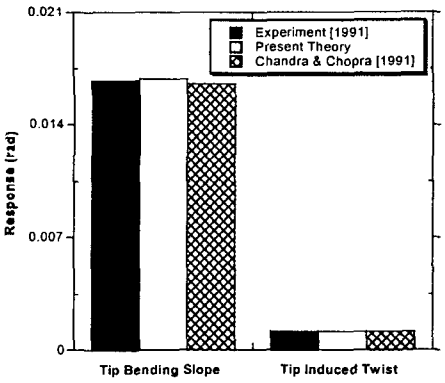

Fig. 7 Comparison of response for bending-torsion coupled blade (Blade 3) under unit tip bending load.

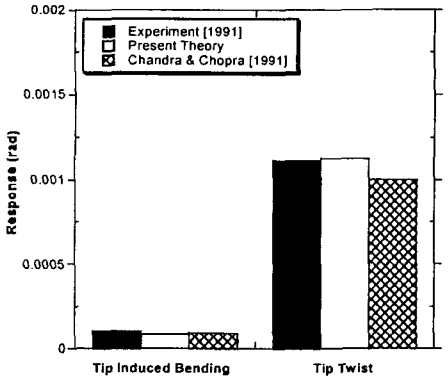

Fig. 8 Comparison of response for bending-torsion coupled blade (Blade 3) under unit tip torque load.

Table. 1 Geometry and material properties of composite blades.

Properties	Values	Dimension	Values
E_{11}	131 GPa (19×10^6 psi)	Airfoil type	NACA 0012
E_{22}	9.3 GPa (1.35×10^6psi)	Length	641.4 mm (25.25 in)
G_{12}	5.86 GPa (0.85×10^6psi)	Chord	76.2 mm (3 in)
ν_{12}	0.40		
Ply thickness	0.127 mm (0.005 in)	Airfoil thickness	9.144 mm (0.36 in)

Table. 2 Lay-up cases of bending-torsion coupled composite blades.

Cases	Spar		Web	Skin
	Top Flange	Bottom Flange		
Blade 1	$[0/15]_4$	$[0/-15]_4$	$[0/\pm 15/0]_2$	$[15/-15]$
Blade 2	$[0/30]_4$	$[0/-30]_4$	$[0/\pm 30/0]_2$	$[30/-30]$
Blade 3	$[0/45]_4$	$[0/-45]_4$	$[0/\pm 45/0]_2$	$[45/-45]$